

# Sokół et al., 2021

## Supplementary Material

### Contents

<b>FIELD AND PETROGRAPHIC EXPRESSION</b> .....	1
<b>ISOCON METHOD CALIBRATION AND DISCUSSION OF LIMITATIONS</b> .....	6
<b>MODELLING BULK HFSE-MASS – GEOMETRIES AND PARAMETERS</b> .....	9
<b>REFERENCES</b> .....	13

### **FIELD AND PETROGRAPHIC EXPRESSION**

The sampling of fenite involved performing of several traverses on km-scale away from the intrusion contact in the NNE-SSW direction towards the unaltered Eriksfjord exposure, which was compounded with samples collected in the N-S direction within the proximal aureole. Several sampling traverses were also done on m-scale in the NNW-SSE orientation across the Igaliku dykes (i.e. at 1 and ~2 km distance, see Fig. 1B) to evaluate the local impact of a couple major dyke swarm bodies (IDS in Fig. 1B).

The Illerfissalik-related fenite after Eriksfjord arenite at Narsaarsuk is typified by the loss of most primary sedimentary textures and thermal induration. The Eriksfjord arenite is typically white or reddish with reduction spots (e.g. Sillisit, S Qassiarsuk; Tirsgaard & Øxnevad, 1998; see also GEUS, 2013 for colour photography) but in the fenite, secondary hues of green, blue, red and pale yellow replace the common original white or red pigment (Fig. 1C) due to growth of perthitic feldspar and pyroxenes and amphiboles (Fig. 1E). The mafic minerals are found as podiform clusters, in veins and lining along the relict sedimentary foresets (Fig. 1D). Ca-pyroxene-rich selvages commonly develop separating feldspar and titanite-rich vein cores from the country rocks, while feldspar is more broadly disseminated throughout the fenite matrix. Pseudofoliation fabric develops locally at m-scale (resorption of solids also visible in thin-section), suggesting country rock rheomorphism (e.g. Goodspeed, 1952; Mehnert, 1968) and relatively high-T conditions in the aureole driving textural change in specific parts of stratigraphy.

Curved interlobate and near-ameboidal fenite matrix microstructures and quartz grain boundary attitudes (Fig. DR1.1b-g) suggest a relatively hot aureole environment (>600°C) with quartz recrystallizing by grain-boundary migration at high-temperature and low strain rate (cf. Passchier & Trouw, 2005). Individual mineral microstructures (i.e. in metasomatic mesoperthite, classified according to Parsons et al., 2015; Fig. DR1.1h, i) suggest an accordingly hot magmatic fluid medium. The metasomatic feldspar is found throughout the proximal zone filling interstices irrespective of

investigated position in succession providing evidence for widespread pervasive alteration. Rocks show no significant overprint by retrograde processes and comprise a calc-silicate assemblage reminiscent of relatively high-T (~500-800°C) skarns (Einaudi et al., 1981; Meinert, 1992; Meinert et al., 2005), here free of often characteristic garnet, epidote, scapolite etc. and forming upon a limestone-free protolith.

Fenite and other alteration styles are usually classified based on the ‘intensity’ of textural or mineralogical change. As no consistent scheme yet exists for products of alkali metasomatism in carbonatitic-alkaline settings, the qualitative ‘grade’ classification of Morogan (1994) is preferred:

- Low-grade fenites (LGF) – textures and mineralogy inherited from the protolith present and largely unaltered
- Medium-grade fenites (MGF) – relicts rare, new rock textures develop from fluid injection and by replacement reactions or recrystallisation
- High-grade fenites (HGF) - primary mineralogy almost fully consumed, flow-banding and igneous-like appearance common attesting to recrystallisation of remobilised solids by the fenitising fluid

The relict sedimentary structures present at N Narsaarsuk (Fig. 1D) determine the overall maximum grade to be no higher than ‘medium’ in this scheme and no syenites of metasomatic origin were noted within the transition across the Illerfissalik-Eriksfjord contact.

Table DR1.1 – Mineralogy summary and sample information for the fenite in the Narsaarsuk aureole and its protolith in Fig. DR1.1

	<b>Sample</b>	<b>Eastings</b>	<b>Northing</b>	<b>Main minerals (&gt;5% mode, in order of abundance)</b>	<b>Accessory (&lt;5% mode)</b>
a	KSL-10- 2b	61.03417 (477608.9)	-45.41444 (6766664)	Qz ± Hem*	Afs, Hem, Bt, Lm
b, c	KSL-2-3c	61.04028 (478783.2)	-45.39278 (6767337)	Qz, Afs (occasionally poikilitic with Aeg), Di, Bt	Ri, Ttn, Ap ± Zrn
d, f	KSL-5-4a	61.03528 (478779.8)	-45.39278 (6766781)	Afs, Di, Qz, Ri, Ktp	Bt, Ap, Ttn, Zrn, Cal, Hem ± Wo
e, g, i	KSL-14- 3a	61.02750 (479119.9)	-45.38639 (6765912)	Qz, Afs (invariably poikilitic with Aeg), Ri	Bt, Ttn, Nyb, Hem, CGM, Mzt, Ap, Bzr
h	KS19-5-1	61.01144 (480144.2)	-45.36725 (6764117)	Qz, Afs, Ri	Bt, Hem

GPS coordinates provided in decimal degree format and UTM Zone 23N to cross-reference with Fig. 1B in the main text

Modal abundances determined by point counting (usually 500 counts, except for exceptionally homogeneous quartzites), see also Table DR1.3. Statistics available from the author on request.

Mineral abbreviations following IUGS Subcommittee recommendations for metamorphic rocks (Siivola & Schmid, 2007): quartz (Qz), hematite (Hem), alkali feldspar (Afs), biotite (Bt), limonite (Lm), aegirine (Aeg), diopside (Di), richterite (Na-Ca amphibole, Ri), titanite (Ttn), apatite (Ap), zircon (Zrn), katophorite (Na-Ca amphibole, Ktp), calcite (Cal), wollastonite (Wo), nybøite (Na-amphibole, Nyb), chevkinite-group-minerals (CGM), monazite (Mzt), bazirite (Bzr)

Sample 5-1 collected further ~1 km south of S Narsaarsuk region along the contact towards Iganaq between Illerfissalik summit and the tip of the Igaliku Fjord (see also accounts of Emeleus & Harry, 1970; Pearce, 1988 referenced in the main text), however fenite textures and the Eriksfjord protolith are analogous.

Samples 2-3c and 14-3a correspond to fenite shown in Fig. 1D-E of the main text

\* Hematite listed twice for 10-2b due to relative variability in the Illiortarfik area where strongly hematised, BIF-like areas, or outcrops broadly similar to those at Sillisit, can occur

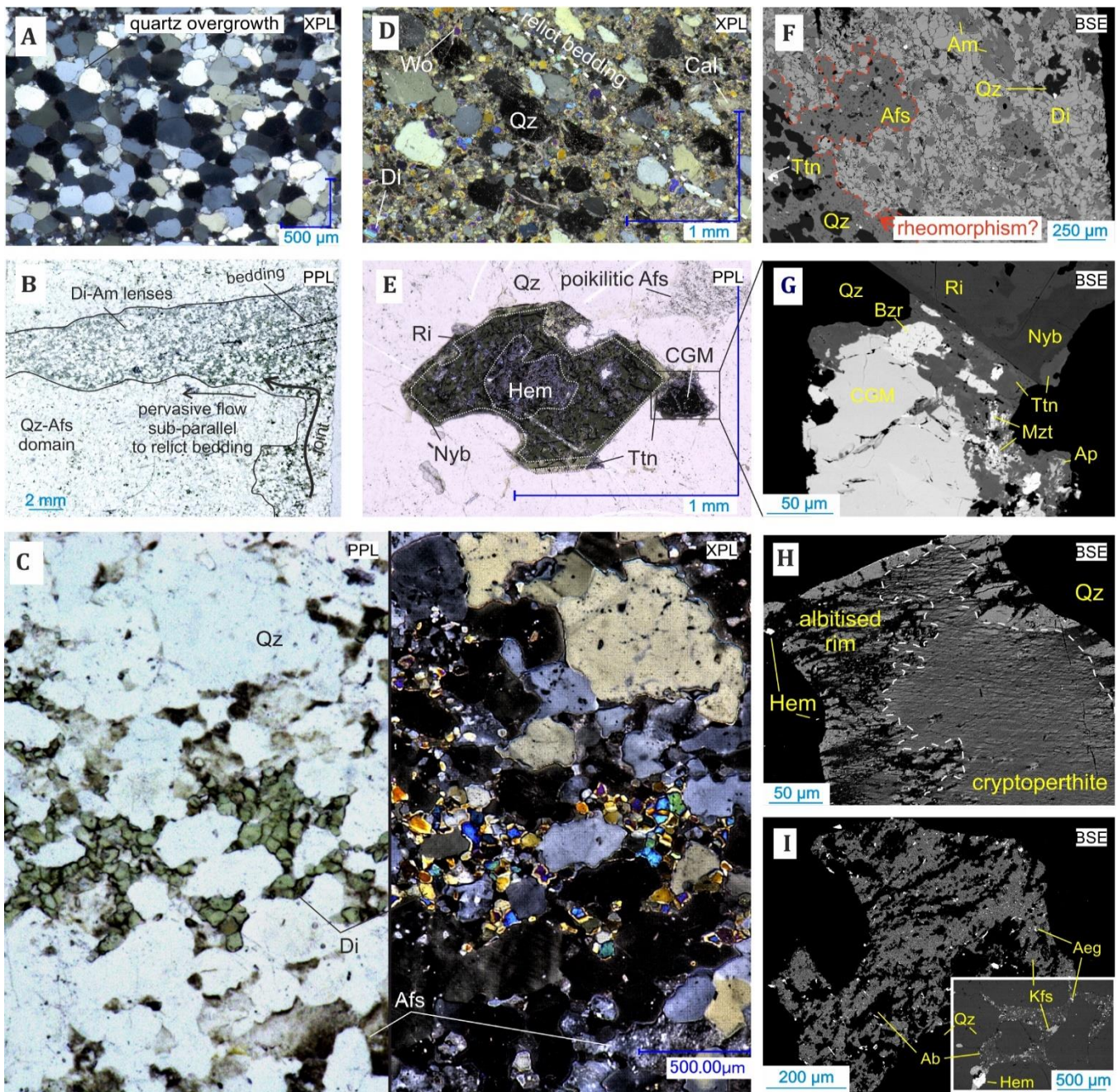


Figure DR1.1 – textural characteristics of the Eriksfjord arenite (Fig. 1A) and the subsequent Illerfissalik fenite (Fig. 1B, 1C) determined by optical (a-e) and backscatter electron microscopy (f-i); a) the quartz arenite protolith; b-i) Illerfissalik fenite; the figure showcases evidence for:

- pervasive (along grain boundaries) and structure-hosted (i.e. along joints and bedding) fenitizing fluid flow (b-c)
- significant interaction with a Ca-rich high-T fluid based on the secondary calc-silicate mineralogy, remobilisation of primary silica and the embayed mineral terminations (d, f)
- multiple generations of fenitizing fluid causing formation of reaction rims and outer Na-rich zones upon pre-existing Na-Ca amphiboles (e-g) and feldspars (h)
- the presence of secondary HFSE-hosting minerals i.e. CGM (e-g)
- deuteric recrystallisation of secondary high-T crypto- (h), meso- (i) and the often coexisting antiperthite (inset in i), often in a flame-perthite habit

Further modal mineralogy detail and the corresponding sample information in Table DR1.1. Amphibole end members determined from EPMA data using the Locock (2014) spreadsheet. Mineral abbreviations follow the IUGS Subcommittee recommendations for metamorphic rocks (Siivola & Schmid, 2007), several uncommon minerals: CGM = chevkinite-group minerals (Macdonald et al., 2019), bzt = bazirite (Ba-variant of wadeite Zr-silicate)

## WHOLE-ROCK METHODOLOGY

All samples were split and pulverised at the University of St Andrews using a conventional jaw crusher and tungsten carbide ring mill (2 minutes of milling, or longer in the case of syenite) to a uniform particle size <150  $\mu\text{m}$ . The assay data were obtained for major elements at Bureau Veritas labs in Vancouver, Canada (BVC) by  $\text{LiBO}_2/\text{Li}_2\text{B}_4\text{O}_7$  fusion using inductively coupled plasma atomic-emission spectrometry (ICP-AES; BVC analytical code LF300). Trace elements for the I4 intrusion samples were analysed for at the University of St Andrews (STA) by X-ray fluorescence (XRF) on pellets steel-pressed with FLUXANA CEREOX binding agent. Fenite and protolith were analysed by ICP-AES and mass spectrometry (ICP-MS) for major and trace elements by  $\text{LiBO}_2$  fusion prior to acid dissolution at ALS Geochemistry, Loughrea, Ireland (analytical codes ME-ICP06 and ME-MS81d).

Accuracy and precision were tested using several internal (SO-19 @ BVC) and certified reference materials (GSP2 granodiorite @ STA; SY-4 syenite, REE-1, OREAS 102a, AMIS0304 @ ALS) - see Table DR1.2 and the source data within the Supplementary Dataset DR2.1. Replicates were analysed at BVC and ALS – data were within the  $2\sigma$  error of the results from all labs confirming no systematic differences between data from each lab. Blanks from BVC were  $\leq 0.03$  wt% oxide for major elements and below detection for trace elements, and from ALS these were <0.05 wt% oxide and <1 ppm, respectively, indicating no contamination issues.

Table DR1.2 – standardisation summary

	<b>Absolute accuracy (wt% ox. or ppm)</b>	<b>Accuracy relative to certified value (%)</b>	<b>Precision (% RSD)</b>
BVC (ICP-AES, major elements)	<1	<2.6 (<1.5 for components > 1 wt%)	<1 (2.55 for $\text{P}_2\text{O}_5$ only)
STA (XRF, trace elements)	<15	>8 for Sm and U only	>11 for Sm and U only
ALS (ICP-AES, majors)	<0.6	typically <1 (>10 for $\text{Na}_2\text{O}$ , MnO & $\text{Cr}_2\text{O}_3$ )	>1 for $\text{Na}_2\text{O}$ , MnO & $\text{Cr}_2\text{O}_3$ only
ALS (ICP-MS, traces)	>3 for Nd, Y and Ba only	typically <8	>5 for Tm only

## ISOCON METHOD CALIBRATION AND DISCUSSION OF LIMITATIONS

The raw compositional data (see Table DR1) for the fenite compared to unaltered rocks show an increase in all elements except silica  $\leq 400$  m of the Illerfissalik contact. Significant increase ( $\sim 10$  wt%) occurs in  $\text{Al}_2\text{O}_3$ , alkalis and  $\sim 2\text{-}3$  wt% in CaO and MgO, and  $\leq 400$  ppm Sr. Past studies transformed the raw data to a 'standard cell' of 100 anions (typically  $\text{O}^{2-}$ ; McKie, 1966) or developed similar geochemical indices (i.e. IFQ – the chemical fenitization index, as in Rodrigues et al., 2010), which however did not account for several critical physical parameters (Appleyard & Woolley, 1979). To account fully for element mass-transfer considering the physical mass and volume change, statistical analysis is traditionally performed by comparing compositions of the altered and unaltered rocks using the isocon method adapted from the original Gresens (1967) study. The equations (after Grant, 1986) account for rock specific gravity ( $\rho$ ) and volume ( $f_v$ ) changes, which minimise the closure effect (whole-rock data must add up to 100%) arising from standard bulk-rock data analysis (Ague & van Haren, 1996). The change in concentration of a component is calculated using  $[\Delta C_i = ((\frac{m^a}{m^o})(\frac{C_i^a}{C_i^o}) - 1) C_i^o]$ ; where  $m$  and  $C$  refer to the mass and concentration of component  $i$  in altered and original sample (superscript  $a$  and  $o$ ). Once calculated, the change is often divided by the original concentration ( $\Delta C_i/C_i^o$ , as in Grant, 1986) to represent best the degree of alteration, although in some cases only the gains experienced by the wall-rock were deemed pertinent in measuring the impact of metasomatic process (fenitisation index – F.I.; Kresten, 1988). The isocon model requires one of three assumptions be made to define the isocon reference line: (1) no mass change, (2) no volume change, or (3) one or several elements are immobile.

While the task of determining immobile elements is trivial in most silicate crustal systems, qualitative studies of alkaline magmatism commonly show mobility of HFSE and  $\text{Al}_2\text{O}_3$  - components that are ordinarily considered immobile (MacLean & Barrett, 1993). Nevertheless, immobile components can be defined iteratively (i.e. Arzamastsev et al., 2011; Korchak et al., 2011), or by proxy of the Gresens (1967)  $f_v$  curve clustering method where multiple elements with identical  $f_v$  values at 0 gain/loss, indicate both level of volume change and immobility (see Cooper et al., 2016). In the present study, HFSE mobility is evident from the presence of chevkinite-group minerals (CGM; Fig. S1e, g) and Nb-LREE-rich secondary titanite disseminated in the fenitized quartz arenite at Narsaarsuk.

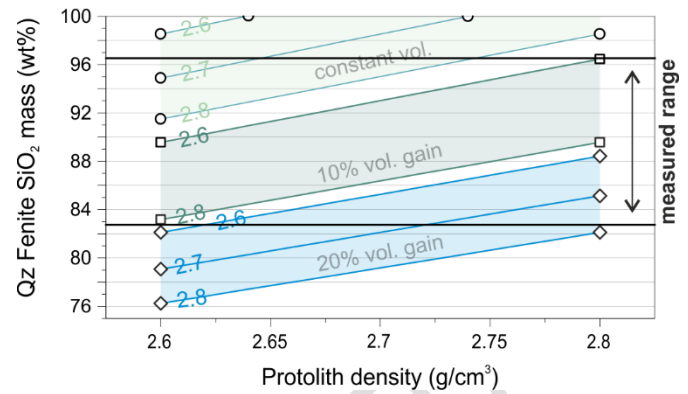


Figure DR1.2 – the effect of volume change and altered rock density (each diagonal) on the measured whole-rock composition in fenite using  $\text{SiO}_2$  example

Examining the different isocons across the fenitized area also shows HFSE i.e. Zr, Y, Ta, Tm are variably mobile, suggesting they are not the ideal reference species.

Due to lack of an immobile reference element, we examined the alternative approaches. We choose to apply the constancy of mass scenario where “one may assume that the sums of components supplied and depleted during fenitization roughly balance, i.e. that the total mass change of the rock during fenitization will be at minimum” (Kresten, 1988; p. 349). It should be noted that in this case  $\text{SiO}_2$  appears to define the CM-isocon (Fig. 2B-2D) implying immobility. Brief examination of the  $f_v$  parameter under these conditions shows the preservation of  $\text{SiO}_2$  mass could be satisfied through volume increase up to ~20% (Fig. DR1.2) in the likely range of fenite and protolith density (2.6-2.8  $\text{g/cm}^3$ ). Contact breccias resulting from expansion do occur at Illerfissalik (best exposed towards mid-to-S Narsaarsuk, Fig. 1B), but outcrops are small (m scale) and discontinuous, leading us to infer volume gain is not widespread. Some leaching must have occurred (based on textural lack of  $\text{SiO}_2$  cement) and we therefore conclude volume loss in this system. We stress however that the measured values cannot be explained by volume change alone and metasomatic exchange is significant.

MANUSCRIPT ACCEPTED

Table DR1.3 – modal mineralogy and the corresponding calculated bulk density (weighted based on mineral composition) of the selected fenite and protolith samples

Category	Fenite	Fenite	Fenite	Fenite	Fenite	Fenite	Fenite	Fenite	Fenite	Fenite	Fenite	Protolith	Protolith	Protolith	
Type	Matrix	Matrix	Matrix (+fine veins)	Matrix	Matrix	Matrix	Vein	Matrix	Matrix	Matrix (+fine veins)	Vein	Matrix	Matrix	Matrix	
Sample #	14-3a	2-3a	2-3c	5-1	6-6	6-6	2v	14-3a	2-3a	2-3c	5-4a	10-5c	10-4a	10-4b	
Method	Pt Count	Pt Count	Pt Count	Pt Count	Pt Count	Estimate	Estimate	Estimate	Estimate	Estimate	Estimate	Pt Count	Pt Count	Pt Count	
<i>Mineral</i>	<i>Density (g/cm<sup>3</sup>)</i>														
Quartz	2.65	85.20	66.80	51.50	82.20	65.60	37.00	60.00	40.00	40.00	35.00	30.00	90.80	84.50	97.30
Alkali Feldspar (Or)	2.55	10.80	22.20	20.10	11.40	30.00	45.00	14.00	30.00	40.00	45.00	20.00		7.20	2.00
Pyroxene (Di)	3.4	0.20	7.00	9.00			7.00	3.00	10.00	7.00	6.00	25.00			
Amphibole (Ri)	3.06	1.80	1.40	4.80	4.80		2.00	10.00	4.00	2.00	2.00	5.00	4.20		
Biotite (Annite)	3.26			8.20			2.00		5.00	5.00	7.00	5.00	2.00		
Titanite	3.47		1.80	1.40		3.20	5.00	6.00	5.00	5.00	4.00	3.00			0.20
Zircon	4.65		0.40	0.60		1.00	2.00	1.00	1.00		0.00				0.20
Epidote	3.45							1.00	1.00		1.00	2.00			
Apatite	3.15			0.40		0.20		2.00	1.00			2.00	0.40		
Calcite	2.71							1.00	2.00			5.00			
Fe-Ti oxides (Hem)	5.3	2.00	0.40	4.00	1.60				1.00	1.00		3.00	2.60	8.30	0.30
Others								2.00							
Total		100.00	100.00	100.00	100.00	100.00	100.00	100.00	100.00	100.00	100.00	100.00	100.00	100.00	100.00
Arithmetic bulk density		2.70	2.72	2.90	2.70	2.67	2.76	2.73	2.84	2.77	2.74	3.00	2.75	2.86	2.66
Subcategory		Fenite (pt counting)						Fenite (estimates)				Protolith			
Mean density		2.74						2.81				2.76			

Mineral abbreviations as in Table DR1.1. Mineral densities as reported on <http://webmineral.com>, assumed solid-solution end-member cited where appropriate.

The final uncertainty in isocon models is the choice of the unaltered reference sample. This is often difficult in cratonic regions where natural protolith variation and taking any arbitrary sample as a reference introduces large  $\Delta C_i/C_i^0$  errors, frequently several orders of magnitude, into the calculations. The Kresten (1988) study attempted to reduce this effect by calculating an average wall-rock composition (AWR) of five samples in the Fen area. Subsequent studies highlighted that this approach is prone to problems as it is often difficult to measure the extent of the aureole and several specimens can be classed as low-grade fenite leading to underestimation of elemental transfer (Verschure & Maijer, 2005). The Eriksfjord quartz arenite, however, we find to be exceptionally well suited for this approach, as it shows no significant lateral variation in facies at the stratigraphic level (Stewart, 1964) and therefore inherent heterogeneity is assumed to be negligible. No protolith samples show >5% modal feldspar or clay, except within ~5 m of regional dyke contacts at >0.4 km distance (Fig. 2D) or where the protolith is strongly hematized (Table DR1.3). The mean whole-rock composition for the protolith population of 15 samples is used here as a reference composition rather than an arbitrary sample due to wide availability of sedimentary exposures, which represent the same formation and likely the same stratigraphic member, across a ~6 km<sup>2</sup> area, which decreases the likelihood of using an extreme composition or that the low-grade alteration signature would be imparted on the result. Density values used in this isocon study are 2.6 and 2.8 g/cm<sup>3</sup> for the protolith and fenite respectively. As a guide, the generalized densities for the protolith and its fenite were calculated from the observed modal compositions of the selected samples (Table DR1.3). Although some relatively denser samples do occur especially where veins (Fig. 1D; pyroxenite 5-4a – Fig. DR1.1D, DR1.1F) or thin veinlets 10 µm to 2 mm wide (i.e. 2v, 2-3c – Fig. DR1.1B; Table DR1.3) cut the fenite otherwise comprised by uniformly dispersed metasomatic mineralogy, or locally in hematite-rich sandstone (i.e. 10-4a; Table DR1.3), the excursions are small and majority of the wall-rock is represented by compositions described in Table DR1.1 and the impact of changing between the values in the stated density range on the output was found to be insignificant.

## **MODELLING BULK HFSE-MASS – GEOMETRIES AND PARAMETERS**

The impact of fenitization on ore genesis in a large, open magmatic system can be shown through attributing compositional data to a scaled 3D geometric model. Our volumetric model was designed for three different geometries of the Illerfissalik centre and three fenite widths (the observed 400 m among those; Fig. DR1.3a-c) to obtain mean HFSE and TREO values representative of the cargo introduced into the wall-rock by the fenitizing fluids. The Data Repository tables DR2.3-2.5 contain calculations for our model, the results of which are summarized in Table DR2.2. For benchmarking purposes, here we also present the same calculation applied to a structurally better constrained Ilímaussaq Complex where it is often assumed that no significant HFSE or volatile loss and isotopic mixing have occurred, and the centre is a world-class magmatic HFSE ore deposit (Larsen & Sørensen, 1987; Marks & Markl,

2015). At Ilímaussaq a narrow (10-200 m; Ferguson, 1964) fenite of similar character (Derrey, 2012) is described and for comparative purposes it is here presented as a relatively ‘closed’ system.

The main models (those interpreted to best represent the true geometry) assume both centres are ellipsoids (Illerfissalik =  $2x \sim 14$  km,  $2y \sim 7.6$  km laterally and  $2z \sim 3-6$  km from base to apex; Ilímaussaq =  $\sim 17$ ,  $9.95$  and  $\sim 1.8$  km respectively, unit thicknesses based on Andersen et al., 1981; Bailey et al., 2001; incl. Black Madonna unit after Schønswandt et al., 2015; Tables DR2.3-2.5) and use only the reported cumulate unit compositions (weighted by unit thickness where appropriate i.e. for Ilímaussaq kakortokite and lujavrite sequences, see Table DR2.5). X and Y dimensions are inferred from the geological map data found in various sources i.e. Upton (2013), Marks & Markl (2015) or the GEUS Greenland Portal.

We model our data to three variants of the Illerfissalik system – 1) an ellipsoid with  $z = 1.5$  km; 2) an ellipsoid with  $z = 3$  km and 3) a cylinder with  $z = 1.5$  km to represent the three most broadly realistic geometries. The fenite shell is calculated for each of these geometries with a 200, 400 and 800 metres strip added (Table DR2.3) to represent the actual observed fenite (400 m) and the plausible min-max range within which the average fenite concentration would still faithfully represent the true, appropriately scaled, gradationally weakening, fenitizing fluid signal (Fig. DR1.3). The volumetric calculation relationship can be described as follows:  $V_{\text{Fenite}} = V_{\text{I4+Fenite}} - V_{\text{I4}}$  and for simplicity it is also assumed that  $V_{\text{Fenite}} = V_{\text{Unaltered Protolith}}$  (Table DR2.3, DR2.4). For Ilímaussaq, similar subtractive calculations were made to calculate the stratified chamber volumes for kakortokite, lujavrite, basal saucer-shaped Black Madonna unit and the naujaite dome sequences. Density of the igneous nepheline syenitic units for both intrusions is set at  $2.7$ , while that of the fenite is kept at  $2.6 \text{ g/cm}^3$ .

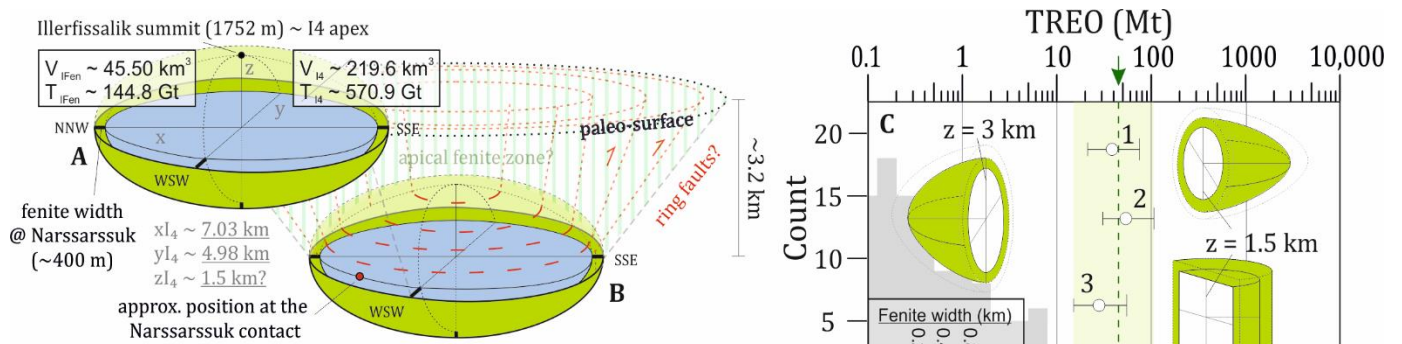


Fig. DR1.3 – (A) diagram showing dimensions of the Illerfissalik (I4) intrusion and its fenite (IFen) shell (here depicted with 400 m observed extent) and the resultant volume (V) and tonnage (T), X and Y based on mapped intrusion extent, length of z < 1.5 km due to max observed exposure of the centre’s magmas at the Illerfissalik summit; (B) schematic representation of the hypothesized fenite zone in the overburden crust above Illerfissalik punctured by conical faults providing conduits for fluid and magma migration, paleo-surface highlighted based on the max extent from the base of Maajuut Formation level in the Eriksfjord Group at which fenite at the Narsarsuk contact is examined

C) TREO mass within Illerfissalik fenite estimated for three different ellipsoidal (1-2, differing by the length of the z-axis) and cylindrical (3, assuming a stock-like shape) geometries of the intrusion+envelope system; error range (green area) defined by the different fenite width for each model, mean value of all models and fenite widths (~43 Mt) denoted by the green line; known deposit data from Fig. 4B highlighted in the background

D) TREO tonnage vs grade comparison of the estimates in this study (Eriksfjord arenite, Illerfissalik I4 syenite and its fenite), simulated comparative Ilímaussaq volumes (pink) and the known deposit data (circles & triangle; from Zhou et al., 2017); green vector indicating the effect of fenitization on bulk TREO grade and tonnage of the modelled Eriksfjord arenite volume

After calculating the rock (or ore) volume we attributed compositional data for the average fenite, protolith, I4 Illerfissalik and Ilímaussaq units to the corresponding ellipsoidal or cylindrical volumes to determine the mass of selected HFSE oxides and TREO within. For this purpose, raw trace element data (in ppm) were converted to oxide form with all REE assumed to be trivalent. Only limited I4 intrusion trace element data by XRF are available, therefore in this study we assume LREO~TREO and whenever comparing the cargo movement, we omit elements such as Ta or Hf which were not detected in the I4 syenite samples. Results are found in Table DR2.4 for Illerfissalik and DR2.5 for Ilímaussaq respectively. Table DR2.6 contains HFSEO data presented in Fig. 4A from both preceding tables arranged by ionic potential. The Ilímaussaq data (Fig. DR1.3d) show that our model estimates the total tonnage in the basal kakortokite unit, which host the Kringleerne deposit in the SE region towards (4.7 Gt @ 0.65 wt% TREO = ~31 Mt; Zhou et al., 2017), at 36.44 Gt @ 0.43 wt% TREO = ~155.7 Mt, indicating the unexposed kakortokite rock volume is ~4x larger – a result we find to be geologically

consistent with the known deposit statistics assuming lopolith-like geometry of the intrusion base. We note that Figure 1.3d should not be confused for the conventional tonnage vs resource grade relationship (i.e. Fig. 3 in Paulick & Machacek, 2017) – it is intended to visualize how fenitization fertilizes the wall-rocks by increasing TREO proportion in the same rock mass.

It should be noted that the simple geometric models applied in this work do not account for many complications expected and unknowns due to lack of public data in such chemically complex magmatic-hydrothermal systems located in an exploration frontier i.e. 3D intrusion and wall-rock compositional heterogeneities, lateral and vertical discontinuity of various units, changing redox conditions, structural traps and several other variables. The volumes and tonnages presented here should not therefore be mistaken for JORC compliant resource estimates. Future workers are therefore recommended to exercise caution when applying a similar approach in geologically complex areas.

MANUSCRIPT ACCEPTED

## REFERENCES

1. Ague, J.J., and van Haren, J.L.M., 1996, Assessing metasomatic mass and volume changes using the bootstrap, with application to deep crustal hydrothermal alteration of marble: *Economic Geology*, v. 91, p. 1169–1182, doi:10.2113/gsecongeo.91.7.1169.
2. Andersen, S., Bohse, H., and Steenfelt, A., 1981, A geological section through the southern part of the Ilímaussaq intrusion: *Rapport Grønlands Geologiske Undersøgelse*, v. 103, p. 39–42, [https://data.geus.dk/gg\\_detail/?cat=rap&id=93051](https://data.geus.dk/gg_detail/?cat=rap&id=93051).
3. Appleyard, E.C., and Woolley, A.R., 1979, Fenitization: An example of the problems of characterizing mass transfer and volume changes: *Chemical Geology*, v. 26, p. 1–15, doi:10.1016/0009-2541(79)90026-3.
4. Arzamastsev, A.A., Arzamastseva, L. v., and Zaraiskii, G.P., 2011, Contact interaction of agpaitic magmas with basement gneisses: An example of the Khibina and Lovozero Massifs: *Petrology*, v. 19, p. 109–133, doi:10.1134/S0869591111020032.
5. Bailey, J.C., Gwozdz, R., Rose-Hansen, J., and Sørensen, H., 2001, Geochemical overview of the Ilímaussaq alkaline complex, South Greenland: *GEUS Bulletin*, v. 53, p. 35–53, doi:10.34194/ggub.v190.5172.
6. Cooper, A.F., Palin, J.M., and Collins, A.K., 2016, Fenitization of metabasic rocks by ferrocarnatites at Haast River, New Zealand: *Lithos*, v. 244, p. 109–121, doi:10.1016/j.lithos.2015.11.035.
7. Derrey, I., 2012, Element transport and mineral replacement reactions during contact metasomatism: Effects on the Julianehåb granite induced by the Ilímaussaq intrusion, SW-Greenland [Diplomathesis].
8. Einaudi, M.T., Meinert, L.D., and Newberry, R.J., 1981, Skarn deposits., in *Economic Geology*, v. 75, p. 317–391, doi:10.5382/AV75.11.
9. Ferguson, J., 1964, Geology of the Ilímaussaq alkaline intrusion, South Greenland: *Bulletin Grønlands Geologiske Undersøgelse*, v. 39, p. 82.

10. GEUS, 2013, Mineral deposit research for a high-tech world: Geological excursion to South Greenland, Excursion Guidebook GRE1, in Bergman Weihed, J., Kolb, J., Bartels, A., Borst, A.M., Bohse, H., and Bell, R.-M. eds., 12th SGA Biennial Meeting, Uppsala, Sweden, Geological Survey of Sweden, p. 59.
11. Goodspeed, G.E., 1952, Replacement and Rheomorphic Dikes: *The Journal of Geology*, v. 60, p. 356–363, doi:10.1086/625983.
12. Gresens, R.L., 1967, Composition-volume relationships of metasomatism: *Chemical Geology*, v. 2, p. 47–65, doi:10.1016/0009-2541(67)90004-6.
13. Korchak, Yu.A., Men'shikov, Yu.P., Pakhomovskii, Ya.A., Yakovenchuk, V.N., and Ivanyuk, G.Yu., 2011, Trap formation of the Kola Peninsula: *Petrology*, v. 19, p. 87–101, doi:10.1134/S0869591111010036.
14. Kresten, P., 1988, The chemistry of fenitization: Examples from Fen, Norway: *Chemical Geology*, v. 68, p. 329–349, doi:10.1016/0009-2541(88)90030-7.
15. Larsen, L.M., and Sørensen, H., 1987, The Ilímaussaq intrusion—progressive crystallization and formation of layering in an agpaitic magma: Geological Society, London, Special Publications, v. 30, p. 473–488, doi:10.1144/GSL.SP.1987.030.01.23.
16. Locock, A.J., 2014, An Excel spreadsheet to classify chemical analyses of amphiboles following the IMA 2012 recommendations: *Computers and Geosciences*, v. 62, p. 1–11, doi:10.1016/j.cageo.2013.09.011.
17. Macdonald, R., Bagiński, B., Belkin, H.E., and Stachowicz, M., 2019, Composition, paragenesis, and alteration of the chevkinite group of minerals: *American Mineralogist*, v. 104, p. 348–369, doi:10.2138/am-2019-6772.
18. MacLean, W.H., and Barrett, T.J., 1993, Lithochemical techniques using immobile elements: *Journal of Geochemical Exploration*, v. 48, p. 109–133, doi:10.1016/0375-6742(93)90002-4.
19. Marks, M.A.W., and Markl, G., 2015, The Ilímaussaq Alkaline Complex, South Greenland, in Charlier, B. ed., *Layered Intrusions*, Springer Geology: Springer Netherlands, p. 649–691, doi:10.1007/978-94-017-9652-1\_14.

20. McKie, D., 1966, Fenitization, in Tuttle, O.F. and Gittins, J. eds., Carbonatites., New York, N.Y., Wiley Interscience, p. 261–294.
21. Mehnert, K.R., 1968, Migmatites and the Origin of Granitic Rocks: Amsterdam, Elsevier.
22. Meinert, L.D., 1992, Skarns and skarn deposits: Geoscience Canada, v. 19, p. 145–162, <https://journals.lib.unb.ca/index.php/GC/article/view/3773>.
23. Meinert, L.D., Dipple, G.M., and Nicolescu, S., 2005, World Skarn Deposits, in One Hundredth Anniversary Volume, Society of Economic Geologists, doi:10.5382/AV100.11.
24. Morogan, V., 1994, Ijolite versus carbonatite as sources of fenitization: Terra Nova, v. 6, p. 166–176, doi:10.1111/j.1365-3121.1994.tb00650.x.
25. Parsons, I., Fitz Gerald, J.D., and Lee, M.R., 2015, Review. Routine characterization and interpretation of complex alkali feldspar intergrowths: American Mineralogist, v. 100, p. 1277–1303, doi:10.2138/am-2015-5094.
26. Passchier, C.W., and Trouw, R.A.J., 2005, Microtectonics: Springer-Verlag, v. 275, 351–353 p., doi:10.1016/S0040-1951(96)00271-5.
27. Paulick, H., and Machacek, E., 2017, The global rare earth element exploration boom: An analysis of resources outside of China and discussion of development perspectives: Resources Policy, v. 52, p. 134–153, doi:10.1016/j.resourpol.2017.02.002.
28. Rodrigues, B., França, Z., and Forjaz, V., 2010, Geochemical evolution in fenitization processes, in Neiva, J.M.C., Ribeiro, A., Victor, M., Noronha, F., and Ramalho, M. eds., Ciências Geológicas: Ensino, Investigação e sua História, Portuguesa de Geólogos Sociedade Geológica de Portugal, p. 261–268. [in Portuguese]
29. Siivola, J., and Schmid, R., 2007, List of Mineral abbreviations: IUGS Subcommittee on the Systematics of Metamorphic Rocks, p. 1–14, papers://32862730-33e4-4f24-9997-a2585c9ed6b6/Paper/p878.
30. Schønwandt, H.K., Barnes, G.B., and Ulrich, T., 2015, A Description of the World-Class Rare Earth Element Deposit, Tanbreez, South Greenland, in Rare Earths Industry: Technological, Economic, and Environmental Implications, Elsevier Inc., p. 73–85, doi:10.1016/B978-0-12-802328-0.00005-X.

31. Stewart, J.W., 1964, The earlier gardar igneous rocks of the Ilimaussaq area of South Greenland [PhD thesis], <http://etheses.dur.ac.uk/9560/>.
32. Tirsgaard, H., and Øxnevad, I.E. i., 1998, Preservation of pre-vegetational mixed fluvio-aeolian deposits in a humid climatic setting: an example from the Middle Proterozoic Eriksfjord Formation, Southwest Greenland: *Sedimentary Geology*, v. 120, p. 295–317, doi:10.1016/S0037-0738(98)00037-2.
33. Upton, B.G.J., 2013, Tectono-magmatic evolution of the younger Gardar southern rift, South Greenland (A. A. Garde, Ed.): *Geol. Surv. Den. Green. Bull.*, v. 29, 1–128 p., doi:10.34194/geusb.v29.4692.
34. Verschure, R., and Majjer, C., 2005, A new Rb-Sr isotopic parameter for metasomatism, and its application in a study of pluri-fenitized gneisses around the Fen ring complex, South Norway: *NGU Bulletin*, v. 445, p. 45–71, [https://www.ngu.no/upload/Publikasjoner/Bulletin/Bulletin445\\_45-71.pdf](https://www.ngu.no/upload/Publikasjoner/Bulletin/Bulletin445_45-71.pdf).
35. Zhou, B., Li, Z., and Chen, C., 2017, Supplementary Materials: Global potential of rare earth resources and rare earth demand from clean technologies: *Minerals*, v. 7, p. 1–9, <http://www.mdpi.com/2075-163X/7/11/203> (accessed November 2020).